Molecular Orbital Analysis of the Intermediates and Products Generated by the Photooxidation of Iron Pentacarbonyl

Paul D. Lyne,† D. Michael P. Mingos,*,‡ Tom Ziegler,§ and Anthony J. Downs†

Inorganic Chemistry Laboratory, South Parks Road, Oxford OX2 6UD, U.K., Department of Chemistry, Imperial College of Science, Technology and Medicine, South Kensington, London SW7 2AY, U.K., and Department of Chemistry, University of Calgary, 2500 University Drive, Calgary, Alberta, Canada T2N 1N4

Received February 3, 1993®

The photooxidation of iron pentacarbonyl by dioxygen in an argon matrix produces a number of intermediates on the way to the generation of the final product, iron trioxide. In this paper we present a theoretical study of the reaction intermediates involved, using the density functional theory (DFT) method. The electronic ground states and geometry optimizations are presented for the five oxoiron carbonyl intermediates, as well as the binary oxides, FeO_2 and $[FeO_3]$.

Introduction

The activation of dioxygen by coordination to a transition metal has been widely studied in recent years.[1] Understanding the transfer of dioxygen from a transition metal to an organic substrate is crucial to understanding both biological[1] and organic[2] oxidation processes. In an attempt to characterize the nature of dioxygen binding to a transition metal, several groups have focused their research interests on the reaction of dioxygen with transition metal carbonyls.[3] Matrix-isolation methods[4] have been used to control and monitor the reaction between metal carbonyl fragments and dioxygen.[5–7] A primary objective of these experiments was to provide an accurate description of oxygen binding to the metal throughout the reaction sequence. Photolysis of $[M(CO)_n]$ in the presence of dioxygen in an argon matrix eventually leads to the formation of metal oxides as final products. However, unsaturated oxo–metal carbonyl species are formed as intermediates, and their structures were characterized by IR spectroscopy in conjunction with isotope enrichment experiments.

Recently Fanfarillo *et al.*[8] have reported their findings of the photooxidation of matrix-isolated iron pentacarbonyl. They identified several transient species during the reaction and proposed the reaction sequence shown in Scheme I. The theoretical studies described in this paper were used to supplement the infrared experimental work and confirm, where possible, the geometries of the intermediates. Density functional theory methods[9] were used to calculate the ground-state geometries of the proposed reaction intermediates. Additionally, thermochemical data for the various reaction steps shown in Scheme I were computed.

Scheme I

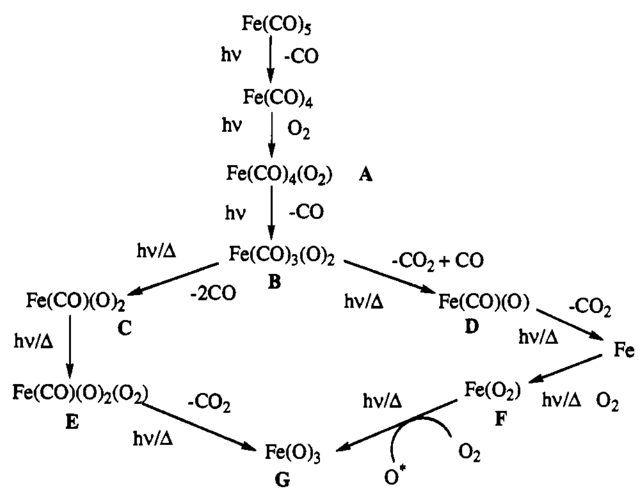

Computational Details

The calculations presented here were carried out using the LCAO-HFS program system developed by Baerends *et al.*[10,11] and vectorized by Ravenek.[12] The numerical integration procedure applied for the calculations was developed by Becke.[13] The geometry optimization procedure was based on the method developed by Versluis and Ziegler.[14] All geometry optimizations were performed in C_{2v} or C_s symmetry. (The optimized geometries of intermediates A and B (see Scheme I) were also found to be at energy minima in C_1 symmetry.) Total energies, E, were evaluated according to eq 1.

$$E = E_{HFS} + E_c + E_x^{NL} + E_c^{NL} \quad (1)$$

† Inorganic Chemistry Laboratory.
‡ Imperial College of Science.
§ University of Calgary.
® Abstract published in *Advance ACS Abstracts*, September 15, 1993.

(1) (a) *Molecular Mechanisms of Oxygen Activation*; Hayasishi, O., Ed.; Academic Press: New York, 1974. (b) *Oxidases and Related Redox Systems*; King, T. E., Mason, H. S., Morrison, M., Eds.; Pergamon: Oxford, England, 1982. (c) *Oxygen Complexes and Oxygen Activation by Transition Metals*; Martell, A. E., Sawyer, D. T., Eds.; Plenum Press; New York, 1988. (d) *Metal Ion Activation of Dioxygen*: *Metal Ions in Biology*; Spiro, T. G., Ed.; Wiley-Interscience: New York, 1980; Vol. 2. (e) Ingraham, L. L.; Meyer, D. L. *Biochemistry of Dioxygen* (*Biochemistry of the Elements*, Vol. 4; Frieden, E., Series Ed.); Plenum Press: New York, 1985.
(2) Sheldon, R. A.; Kochi, J. K. *Metal-Catalysed Oxidations of Organic Compounds*; Academic Press: New York, 1981.
(3) (a) Chambers, R. C.; Hill, C. L. *Inorg. Chem.* **1989**, *28*, 2509. (b) Bilgrien, C.; Davis, S.; Drago, R. S. *J. Am. Chem. Soc.* **1987**, *109*, 3786. (c) Lawson, H. J.; Atwood, J. D. *J. Am. Chem. Soc.* **1989**, *111*, 6223. (d) van Asselt, A.; Trimmer, M. S.; Henling, L. M.; Bercaw, J. E. *J. Am. Chem. Soc.* **1988**, *110*, 8254.
(4) Almond, M. J.; Downs, A. J. *Spectroscopy of Matrix Isolated Species*; Wiley: Chichester, U.K., 1989.
(5) Poliakoff, M.; Smith, K. P.; Turner, J. J.; Wilkinson, A. *J. Chem. Soc., Dalton Trans.* **1982**, 651.
(6) Crayston, J. A.; Almond, M. J.; Downs, A. J.; Poliakoff, M.; Turner, J. J. *Inorg. Chem.* **1984**, *23*, 3051.
(7) (a) Almond, M. J.; Crayston, J. A.; Downs, A. J.; Poliakoff, M.; Turner, J. J. *Inorg. Chem.* **1986**, *25*, 19. (b) Almond, M. J.; Downs, A. J. *J. Chem. Soc., Dalton Trans.* **1988**, 809.
(8) (a) Fanfarillo, M.; Cribb, H. E.; Downs, A. J.; Greene, T. M.; Almond, M. J. *Inorg. Chem.* **1992**, *31*, 2962. (b) Fanfarillo, M.; Downs, A. J.; Greene, T. M.; Almond, M. J. *Inorg. Chem.* **1992**, *31*, 2973.
(9) Ziegler, T. *Chem. Rev.* **1991**, *91*, 651.
(10) Baerends, E. J.; Ellis, D. E.; Ros, P. *Chem. Phys.* **1983**, *2*, 41.
(11) Baerends, E. J. Ph.D. Thesis, Vrije Universiteit, Amsterdam, 1975.
(12) Ravenek, W. In *Algorithms and Applications on Vector and Parallel Computers*; Riele, H. J. J., Dekker, Th. J., van der Vorst, H. A., Eds.; Elsevier: Amsterdam, 1987.
(13) Becke, A. D. *J. Chem. Phys.* **1988**, *88*, 322.
(14) Versluis, L.; Ziegler, T. *J. Chem. Phys.* **1988**, *88*, 322.

0020-1669/93/1332-4785$04.00/0

Here E_{HFS} is the total statistical energy expression for the Hartree–Fock–Slater (HFS) or Xα method[15] while E_c, E_x^{NL}, and E_c^{NL} are additional correction terms. The first correction term, E_c, is a correlation potential for electrons of different spins in Vosko's parameterization[16] from electron gas data. The second correction term, E_x^{NL}, proposed by Becke,[17] is a nonlocal exchange correction to E_{HFS}. Finally, E_c^{NL} is a nonlocal correction to the correlation energy, proposed by Perdew.[18] All bond energies were calculated by the generalized transition state method developed by Ziegler and Rauk[19,20] or by the energy difference between the parent complex and the separated fragments at a long distance apart. The molecular orbitals were expanded as a linear combination of Slater type orbitals (STO).[21] An uncontracted triple-ζ STO[22] basis set was employed for the 3s, 3p, 3d, 4s, and 4p orbitals of iron, whereas 2s and 2p on carbon and oxygen were represented by a double-ζ STO[22] basis set. The ligand basis was augmented by a single STO polarization function, 3d, on carbon and oxygen (ζ_{3d}^{C} = 2.5, ζ_{3d}^{O} = 2.0). The 3s, 3p, 3d, 4s, and 4p orbitals on iron and the upper *n*s and *n*p shells of carbon and oxygen were considered as valence orbitals. The orbitals in shells of lower energy were considered as core and frozen according to the method of Baerends *et al.*[10] A set of auxiliary[23] s, p, d, f, and g STO functions, centered on all nuclei, was used in order to fit the molecular density and present Coulomb and exchange potentials accurately in each SCF cycle. The exchange factor[12,21] α_{ex} in the expression for E_{HFS} was given a value of $^2/_3$ in accordance with Becke's theory.[13] Studies of metal carbonyls[24] have shown that the calculations based on the energy expression given in eq 1 afford metal–ligand energies of chemical accuracy (i.e. ±5 kcal mol^{-1}). Approximate density functional methods have also been tested in connection with conformational energies[25] and triplet–singlet energy separations.[26] More than 50 molecular structures optimized by approximate density functional theory have been compared with experimental structures.[14] The agreement between experimental and approximate density functional structure is, in the majority of cases, excellent.

Results and Discussion

Generation of [Fe(CO)$_4$] and [Fe(CO)$_4$(O$_2$)]. The first step in the reaction sequence for the photooxidation of iron pentacarbonyl is the generation of the transient [Fe(CO)$_4$] molecule. This seemingly innocuous complex has stimulated a great degree of interest in the literature.[27] The main origins of the interest are 2-fold. First, [Fe(CO)$_4$] has been shown to be an intermediate in several organometallic reactions and therefore its investigation provides valuable information about its action. Second, there has been speculation about the exact ground-state electronic structure of this molecule. Initial molecular orbital arguments[28] proposed that the complex could feasibly have a triplet ground state with a C_{2v} structure similar to that proposed from experimental data. The triplet state was predicted to be more stable than the singlet ground state by an *ab initio* calculation

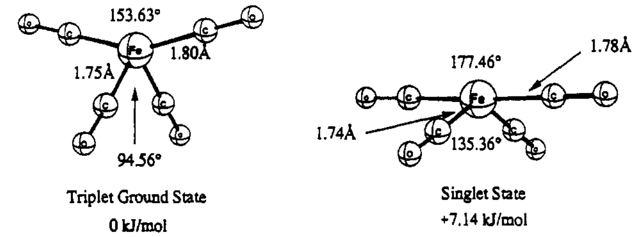

Figure 1. Optimized structures of the triplet (^{3}B$_2$) and singlet. (^{1}A$_1$) electronic states of [Fe(CO)$_4$].

performed by Daniel *et al.*[29] However, Ziegler *et al.*[30] reported that the triplet and singlet states were very similar in energy with the singlet being slightly more stable. Experimentalists have been unable to provide conclusive evidence to resolve this problem. However, there appears to be a consensus in the literature that the triplet state is the ground-state electronic structure of [Fe(CO)$_4$]. It is not possible to record an electron spin resonance spectrum to confirm the paramagnetic nature of the ground state, but Barton *et al.* have qualitatively shown [Fe(CO)$_4$] to be paramagnetic using MCD measurements.[31] In view of the interest in [Fe(CO)$_4$] in the literature and in view of its role as the starting reactive intermediate in the photooxidation of [Fe(CO)$_5$], we chose to optimize its geometry and calculate the energy difference between the triplet and singlet electronic states.

Removal of a carbonyl from [Fe(CO)$_5$] will produce the fragment **1** which will relax to the ground state structure by altering the values of the angles α and β. We have chosen to remove an axial carbonyl.

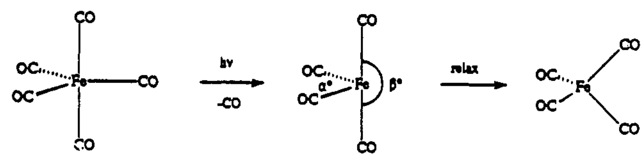

1

The optimized geometries for the $^1A_1$ singlet state with the electronic configuration $(1a_2)^2(1b_1)^2(1a_1)^2(1b_2)^2$ and the ^{3}B$_2$ triplet state with an electronic configuration of $(1a_2)^2(1b_1)^2(1a_1)^2(1b_2)^1(2a_1)^1$ are shown in Figure 1. The frontier orbitals of **1** are well documented.[32]

The triplet structure is seen to be a distorted tetrahedral geometry in agreement with the geometry predicted from experimental data by Poliakoff and Turner.[33] The calculated geometry agrees with that deduced previously by Ziegler *et al.*[30] but differs considerably from that deduced by Veillard *et al.*[29] The singlet ground-state geometry is essentially a trigonal bipyramid with a missing equatorial vertex. We find the total energies of the singlet and triplet electronic states to be very similar with the triplet state being more stable by 8 kJ mol^{-1}.

The enthalpic change, ΔH, for the dissociation of a carbon monoxide molecule from [Fe(CO)$_5$] was calculated using the transition state method developed by Ziegler *et al.* The reader is referred to a recent review by Ziegler[34] for a detailed description of this method. The first ligand dissociation energy can be

(15) Slater, J. C. *Adv. Quantum Chem.* **1972**, *6*, 1.
(16) Vosko, S. H.; Wilk, L.; Nusair, M. *Can. J. Phys.* **1980**, *58*, 1200.
(17) Becke, A. D. *J. Chem. Phys.* **1986**, *84*, 4524.
(18) (a) Perdew, J. P. *Phys. Rev. Lett.* **1985**, *55*, 1655. (b) Perdew, J. P. *Phys. Rev.* **1986**, *B33*, 8822. (c) Perdew, J. P.; Wang, Y. *Phys. Rev.* **1986**, *B33*, 8800.
(19) Ziegler, T.; Rauk, A. *Theor. Chim. Acta* **1977**, *46*, 1.
(20) Ziegler, T. Ph.D. Thesis, University of Calgary, Calgary, Canada, 1978.
(21) (a) Baerends, E. J.; Ros, P. *Int. J. Quantum Chem.* **1978**, *S12*, 169. (b) Baerends, E. J.; Snijders, J. G.; de Lange, C. A.; Jonkers, G. In *Local Density Approximations in Quantum Chemistry and Solid State Physics*; Dahl, J. P., Avery, J., Eds.; Plenum: New York, 1984.
(22) (a) Snijders, G. J.; Baerends, E. J.; Vernooijs, P. *Atom. Nucl. Data Tables* **1982**, *26*, 483. (b) Vernooijs, P.; Snijders, G. J.; Baerends, E. J. Slater-type basis functions for the whole periodic system. Internal Report; Free University: Amsterdam, The Netherlands, 1981.
(23) Krijn, J.; Baerends, E. J. Fit functions in the HFS-method. Internal Report (in Dutch); Free University: Amsterdam, The Netherlands, 1984.
(24) Ziegler, T.; Tschinke, V.; Ursenbach, C. *J. Am. Chem. Soc.* **1987**, *109*, 4825.
(25) Versluis, L.; Ziegler, T.; Baerends, E. J.; Ravenek, W. *J. Am. Chem. Soc.* **1989**, *111*, 2018.
(26) Ziegler, T.; Rauk, A.; Baerends, E. J. *Theor. Chim. Acta* **1977**, *43*, 261.
(27) Poliakoff, M.; Weitz, E. *Acc. Chem. Res.* **1987**, *20*, 408 and references therein.
(28) (a) Burdett, J. K. *J. Chem. Soc., Faraday Trans. 2* **1974**, *70*, 1599. (b) Elian, M.; Hoffmann, R. *Inorg. Chem.* **1975**, *14*, 1058.
(29) Daniel, C.; Benard, M.; Dedieu, A.; Wiest, R.; Veillard, A. *J. Phys. Chem.* **1984**, *88*, 4805.
(30) Ziegler, T.; Tschinke, V.; Fan, L.; Becke, A. D. *J. Am. Chem. Soc.* **1989**, *111*, 9177.
(31) Barton, T. J.; Grinter, R.; Thomson, A. J.; Davies, B.; Poliakoff, M. *J. Chem. Soc., Chem. Commun.* **1977**, 841.
(32) Albright, T. A.; Burdett, J. K.; Whangbo, M.-H. *Orbital Interactions in Chemistry*; Wiley: New York, 1985.
(33) Poliakoff, M.; Turner, J. J. *J. Chem. Soc., Dalton Trans.* **1974**, 2276.
(34) Ziegler, T. *A General Energy Decomposition Scheme for the Study of Metal-Ligand Interactions in Complexes, Clusters and Solids*; NATO ASI C378; Kluwer: Boston, MA, 1992.

Table I. Contributions (kJ mol^{-1}) to ΔH for the Dissociation of CO from $[Fe(CO)_5]$[a]

$\Delta E°$	ΔE_{prep}	ΔE_{a_1}	ΔE_{b_1}	ΔE_{b_2}	ΔE_{orb}
307.9	10.7	–216.9	–79.2	–121.4	–521.4

[a] $\Delta E_{orb} = \Delta E_{a_1} + \Delta E_{b_1} + \Delta E_{b_2}$ including Becke and Perdew corrections.

decomposed as follows:

$$\Delta H = \Delta E° + \Delta E_{prep} + \Delta E_{a_1} + \Delta E_{b_1} + \Delta E_{b_2} \qquad (2)$$

Here $\Delta E°$ is the steric repulsion energy between the carbon monoxide molecule and the $[Fe(CO)_4]$ fragment. The steric repulsion energy has two components. The first is the pure electrostatic interaction, E_{elst}, between carbon monoxide and $[Fe(CO_4]$, and the second, the exchange repulsion energy, ΔE_{exrp}, corresponds to destabilizing two-orbital–four-electron interactions between the fragments.[34]

$$\Delta E° = E_{elst} + \Delta E_{exrp} \qquad (3)$$

The ΔE_{a_1} term represents the contribution to ΔH due to the donation from σ_{CO} to the LUMO of $[Fe(CO)_4]$, and ΔE_{b_1} and ΔE_{b_2} represent back-donation from the metal to the antibonding orbitals of the carbonyl ligand. The ΔE_{prep} term accounts for the energy required to promote $[Fe(CO)_4]$ from its ground-state geometry to the geometry that it adopts in $[Fe(CO)_5]$ with a singlet electronic configuration. The appropriate values are represented in Table I.

The values for the various orbital contributions do not include Becke or Perdew corrections, but they are presented to illustrate the relative magnitudes of the orbital interactions since their *relative* values are independent of corrections. The ΔE_{orb} component refers to the total orbital interaction including Becke and Perdew corrections. This is the value used in the calculation of ΔH.

The energy required to promote $[Fe(CO)_4]$ from the ground-state $^3B_2$ geometry to a singlet state with the geometry adopted in $[Fe(CO)_5]$ is quite low (10.7 kJ mol^{-1}). The synergic interactions are seen to be reasonably well balanced. Our calculations give a ΔH of 203.0 kJ mol^{-1}, which is slightly higher than previous calculated values[24] (ΔH = 185 kJ mol^{-1}). This difference may be attributed to the use of nonlocal corrections different from those used previously.

The next stage in the reaction sequence is the coordination of dioxygen to the unsaturated $[Fe(CO)_4]$ moiety. Fanfarillo *et al.*[8] in their spectroscopic analysis propose that the intermediate A is an η^2-O_2 adduct of $[Fe(CO)_4]$. This form of coordination of dioxygen to iron is in marked contrast with the more familiar end-on monodentate coordination found in biological complexes.[1] Nonetheless, there are examples of d^8 complexes containing the dioxygen ligand that have been structurally characterized as having a distorted octahedral geometry, with dioxygen binding to the metal side-on. The geometry of the molecule $[Fe(CO)_4(O_2)]$ was optimized within the C_{2v} point group. In the original experimental paper, Fanfarillo *et al.* considered two alternatives for the possible structure of the tetracarbonyl fragment in this molecule, one based on C_{2v} symmetry and the other based on C_s symmetry. These are depicted here as **2** and **3**. Fragment **2** is

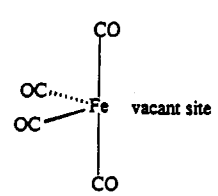

2

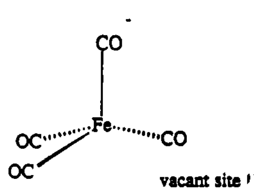

3

essentially derived from a trigonal bipyramid with a vacant site in the equatorial plane. By contrast, the **3** fragment may be seen to be derived from a square pyramid with a vacant site in the basal plane. There is evidence in the literature for both coordination geometries. Matrix-isolation studies of $HMn(CO)_4$ and $CH_3Mn(CO)_4$[35] have suggested that the tetracarbonyl moiety assumes a square pyramidal-based geometry in the molecule. Similar studies of the complexes $XMn(CO)_4$ (X = Cl, Br, I)[36] suggest that the tetracarbonyl fragment adopts a trigonal bipyramidal based geometry. In view of the data for d^8 dioxygen complexes we initially chose to optimise the geometry of $[Fe(CO)_4(O_2)]$ in the C_{2v} point group, and subsequently investigated possible distortions towards a structure based on a square pyramid.

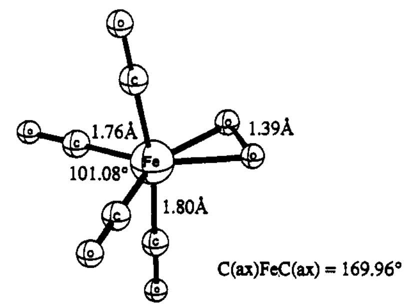

Single Ground State

Figure 2. Optimized structure of $[Fe(CO)_4(O_2)]$.

Our calculations found no evidence for $[Fe(CO)_4(O_2)]$ wishing to attain a square pyramidal based geometry. The fully optimized geometry of $[Fe(CO)_4(O_2)]$ is illustrated in Figure 2 and resembles closely those reported previously for d^8 metal–olefin complexes.

The interactions between the frontier orbitals of $[Fe(CO)_4]$ and O_2 are shown in Figure 3.

The frontier orbitals of dioxygen which are of greatest importance to the interaction with $[Fe(CO)_4]$ are depicted on the right-hand side of Figure 3. There are two fully occupied low-lying π orbitals(π_{a_1} and π_{b_2}) and two high-lying π^* orbitals ($\pi^*_{a_2}$ and $\pi^*_{b_1}$) which are singly occupied. The frontier orbitals of $[Fe(CO)_4]$ are shown on the left-hand side of Figure 3. Reference to the interaction diagram shows that the two main interactions are between the LUMO of $[Fe(CO)_4]$, $2a_1$, and π_{a_1} on oxygen, and between the HOMO of $[Fe(CO)_4]$, b_1, and $\pi^*_{b_1}$ of oxygen. The π_{b_2} and $\pi^*_{a_2}$ orbitals of oxygen do not interact to any great extent with $[Fe(CO)_4]$ and are essentially nonbonding. This poor interaction concerning the a_2 and b_2 sets of orbitals may be attributed to the large energy difference and poor angular overlap between the relevant orbitals. To determine the relative magnitudes of the important interactions in this molecule and the strength of the bond formed between the metal and dioxygen, we used the expression shown in eq 4.

$$D(Fe\text{–}O_2) = \Delta E_{prep} + \Delta E^0 + \Delta E_{a_1} + \Delta E_{b_1} + \Delta E_{b_2} \qquad (4)$$

The preparation energy, ΔE_{prep}, in this case refers to the energy required to distort $[Fe(CO)_4]$ from its ground-state structure to the geometry that it adopts in $[Fe(CO)_4(O_2)]$, with a singlet electronic configuration. Additionally, since the $\pi^*_{b_1}$ orbital of O_2 is vacant in $[Fe(CO)_4(O_2)]$, ΔE_{prep} includes the energy required to bring O_2 from its electronic ground state configuration $^3\Sigma_g^+$ $[(\pi^*_{b_1})^1(\pi^*_{a_2})^1]$ and equilibrium bond distance to the electronic configuration $[(\pi^*_{b_1})^0(\pi^*_{a_2})^2]$ with a bond distance equivalent to the O_2 distance in $[Fe(CO)_4(O_2)]$. The other terms in the equation will have the same meaning as before. The relative importance of back-donation from metal b_1 to $\pi^*_{b_1}$ and of donation from π_{a_1}

(35) (a) Church, S. P.; Poliakoff, M.; Timney, J. A.; Turner, J. J. *Inorg. Chem.* **1983**, *22*, 3259. (b) Horton-Mastin, A.; Poliakoff, M.; Turner, J. J. *Organometallics* **1986**, *5*, 405.
(36) McHugh, T. M.; Rest, A. J.; Taylor, D. J. *J. Chem. Soc., Dalton Trans.* **1980**, 1803.

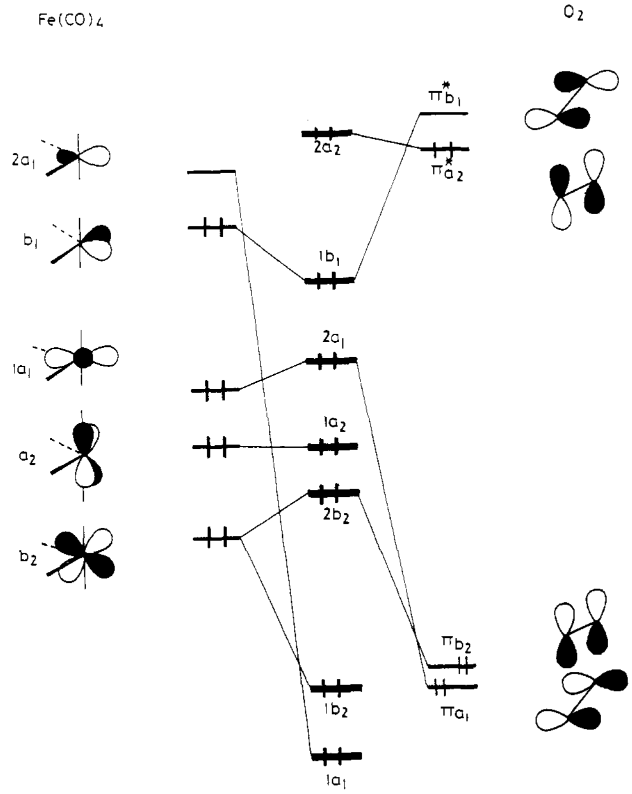

Figure 3. Fragment molecular orbital diagram depicting the interactions between the frontier orbitals of $[Fe(CO)_4]$ and O_2.

Table II. Contributions (kJ mol^{-1}) to ΔH for the Addition of O_2 to $[Fe(CO)_4]$[a]

ΔE°	ΔE_{prep}	ΔE_{a_1}	ΔE_{b_1}	ΔE_{b_2}	ΔE_{orb}
589.6	181.0	−116.7	−612.6	−18.5	−966.9

[a] $\Delta E_{orb} = \Delta E_{a_1} + \Delta E_{b_1} + \Delta E_{b_2}$ including Becke and Perdew corrections.

to $2a_1$ may be assessed by considering the values of ΔE_{a_1} and ΔE_{b_1}. In Table II we present the values for each of the components given in eq 4.

It is found that ΔE_{b_1} far outweighs ΔE_{a_1} and our population analysis indicates that 1.2 electrons are back-donated in total to the dioxygen ligand. These findings are in agreement with previous studies of d^8 dioxygen complexes.[37] Considering the importance of back-bonding in this complex, it is not surprising that the dioxygen distance is 0.2 Å longer than in free dioxygen. The $[Fe(CO)_4]$ fragment has undergone a slight distortion relative to its structure in iron pentacarbonyl. The equatorial angle has closed from 120 to 101° and the axial ligands have bent toward the dioxygen ligand, with a decrease in the angle from 180 to 170°. These slight angular changes, in particular the equatorial distortion, serve to hybridize the lobes of the $2a_1$ and b_1 orbitals on the metal toward dioxygen, thereby enhancing the interactions between the two fragments.

The large electronic stabilizations, ΔE_{a_1} and ΔE_{b_1}, are tempered by the reasonably large energies required to generate the fragments (Table II) and also by the large steric interaction energy, ΔE°, representing in part the destabilizing 4-electron interactions between the $[Fe(CO)_4]$ and O_2 fragments. Evaluation of eq 4 gives the enthalpy change in kJ mol^{-1}. The first excited state, corresponding to a promotion of an electron from the nonbonding $\pi^*_{a_2}$ orbital on O_2, was found to be 33 kJ mol^{-1} less stable.

$[Fe(CO)_3(O)_2]$ and $[Fe(CO)_2(O)_2]$. The second intermediate produced by the photooxidation of $[Fe(CO)_5]$ is postulated by Fanfarillo *et al.* on the basis of spectroscopic data to be $[Fe(CO)_3(O)_2]$. After consideration of $[Fe(CO)_2(O)_2]$ as a candidate for intermediate B,[38] this assignment was reached on the basis of isotopic substitution experiments and a comparison of the experimental spectra with those calculated for a number of different models. There is very little precedent for five-coordinate dioxo–transition metal complexes, and to our knowledge there has never been a structural characterization of a five-coordinate dioxo–iron complex.[39] In contrast, analogues of $[Fe(CO)_2(O)_2]$ are known. The $M(CO)_2(O)_2$ molecule has been previously detected as an intermediate in the photooxidation of group 6 transition metal carbonyls.[5,7] In this section we present our determination of the ground-state structure of $[Fe(CO)_3(O)_2]$. Because of the precedents of the $M(CO)_2(O)_2$ molecule, and the obvious potential role of $[Fe(CO)_2(O)_2]$ in the decomposition of $[Fe(CO)_3(O)_2]$ to $[Fe(CO)(O)_2]$, we also present a study of the $[Fe(CO)_2(O)_2]$ complex.

(37) Norman, J. G., Jr.; Ryan, P. B. *Inorg. Chem.* **1982**, *21*, 3555.

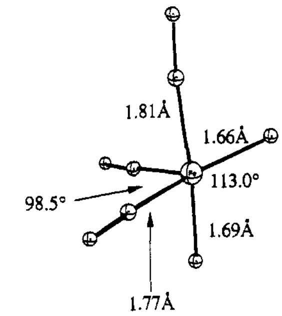

Figure 4. Optimized geometry of $[Fe(CO)_3(O)_2]$.

$[Fe(CO)_3(O)_2]$. Fanfarillo *et al.*[8] propose that $[Fe(CO)_3(O)_2]$ has a distorted trigonal bipyramidal structure with C_s point symmetry. We performed a full geometry optimization restricted calculation on $[Fe(CO)_3(O)_2]$ within the C_s point group. The optimized geometry is shown in Figure 4. Further searches for an energy minimum for the molecule with a triplet and higher spin states were unsuccessful.

Because of the highly distorted geometry of $[Fe(CO)_3(O)_2]$ and the consequent low symmetry of the molecule, the composition and ordering of the frontier orbitals are complex. Initially, we present the frontier orbitals of $[Fe(CO)_3(O)_2]$ with a trigonal bipyramidal geometry and the oxygens *cis* to each other. While this model for $[Fe(CO)_3(O)_2]$ still possesses C_s symmetry and mixing between orbitals on the same center may still occur, the analysis is simpler and helps the frontier orbitals of the optimized structure to be understood. For a D_{3h} ML_5 complex dominated by σ bonding, the frontier orbital manifold is similar to that presented in Figure 5. The 5-fold degeneracy of the metal d orbitals has been split into two doubly degenerate sets and a single a_1 orbital. The lowest lying metal-based orbitals are those whose nodes coincide with the location of the ligands of the trigonal bipyramid. The next set of orbitals corresponds to the degenerate pair of d orbitals lying in the equatorial plane. These interact with the equatorial σ orbitals but hybridize to minimize the unfavorable interactions. Finally, the d_{z^2} orbital lies highest in energy, interacting the most strongly with the ligand orbitals. If we switch on the interactions with the π orbitals on the ligands and have an arrangement of π donors and acceptors consistent with trigonal bipyramidal $[Fe(CO)_3(O)_2]$ (see Figure 5), how are the frontier orbitals altered? Consider the d_{xz}/d_{yz} pair of orbitals that do not interact with the ligand σ orbitals. The d_{yz} orbital overlaps with the apical and equatorial π^* orbitals and the p_y orbital on the axial oxygen. Overall, it overlaps more with the π acceptor orbitals and therefore is stabilized in energy with respect to the case when there are only σ interactions. On the other hand, d_{xz} overlaps with two donor orbitals and only one

(38) Downs, A. J. Unpublished results.
(39) Cambridge Structural Database.

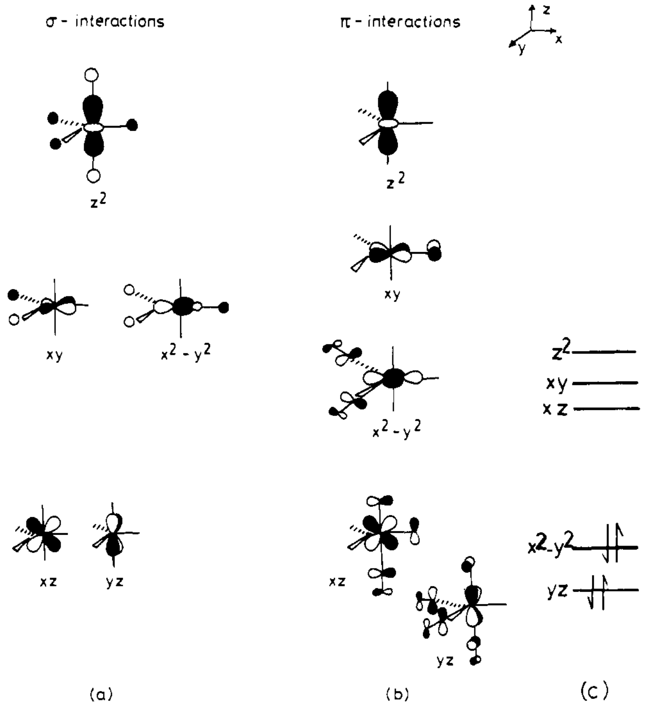

Figure 5. The frontier levels of (a) ML_5 s interactions only, (b) trigonal bipyramidal $[Fe(CO)_3(O)_2]$ with σ and π interactions, and (c) optimized $[Fe(CO)_3(O)_2]$.

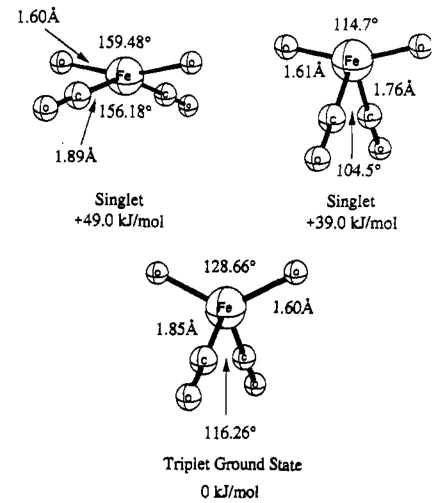

Figure 6. Optimized structures of $[Fe(CO)_2(O)_2]$ located on the C_{2v} energy surface from tetrahedral to square planar geometries.

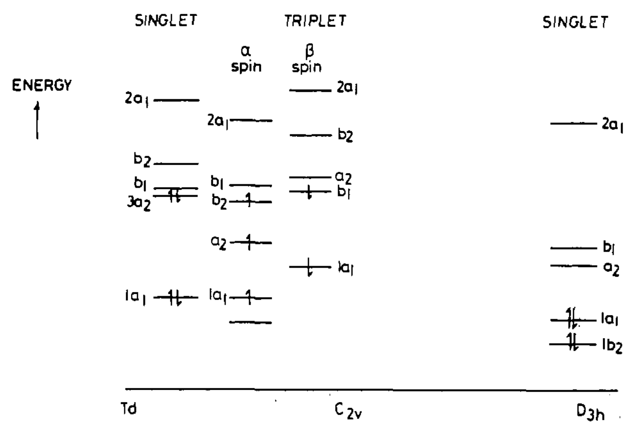

Figure 7. Frontier levels for the optimized structures of $[Fe(CO)_2(O)_2]$.

acceptor orbital, and so there is a net destabilization of the d_{xz} orbital. The next pair of orbitals to consider is the $d_{x^2-y^2}$ and d_{xy} set. From Figure 5 it may be seen that the $d_{x^2-y^2}$ orbital interacts more with π acceptor orbitals and as a result is stabilized. However, the d_{xy} orbital overlaps well with the p_y orbital or the equatorial oxygen. Thus, this orbital is destabilized with respect to its energy in the case where there are only σ interactions. The d_{z^2} orbital does not enter into π interactions with the ligands. In C_s symmetry this simple analysis is complicated by mixing between the metal-based orbitals. The resulting hybridization will modify the arguments developed above, but the energy level orderings are essentially the same. To complete our analysis of the bonding of $[Fe(CO)_3(O)_2]$, we show the energies of the frontier levels in Figure 5. Despite the considerable distortion of the structure from a trigonal bipyramid, and the corresponding effects on the σ and π overlaps, it is possible to understand the energy level ordering of the molecule remembering the respective influences of σ and π interactions on the metal *d* orbitals.

$[Fe(CO)_2(O)_2]$. Our primary aim was to determine the ground-state structure of $[Fe(CO)_2(O)_2]$. Typically, a d^4 ML_4 complex prefers a tetrahedral geometry, whereby the 5-fold degeneracy of the d levels is lifted by the tetrahedral ligand field into a doubly degenerate pair (e) lying below a destabilized triply degenerate set (t_2). Occupation of the lower lying e set by the four metal-based electrons provides the greatest ligand field stabilization for the molecule. However, it is possible to envisage two situations where this picture will need to be modified. First, if the ligands bonded to the metal have a low spectrochemical effect on the metal *d* orbitals, the splitting between the e and t_2 orbitals in the tetrahedral field may be small enough that a high-spin state is preferred to the low-spin $e^4t_2^0$ configuration. Second, the introduction of ligands that are capable of strong π bonding may change the simple splitting pattern expected for a tetrahedral ligand field.

The geometry optimization calculations for this molecule were based on the C_{2v} energy surface. An extensive search along the pathway from a tetrahedron to a square plane was performed for singlet, triplet, and higher spin configurations. We located two minima on the singlet energy surface and one minimum on the triplet energy surface. The optimized geometries are shown in Figure 6. The bond lengths for each of the structures are quite similar, with the Fe—C distance ranging from 1.85 to 1.89 Å and the Fe═O distance constant at 1.60 Å. However, the angular distribution of the ligands about the metal varies considerably, starting with a pseudotetrahedral singlet distorting to a pseudotetrahedral triplet and finally a square planar singlet. The relative total energies of the three states are shown in Figure 6. Not surprisingly, perhaps, the pseudotetrahedral structure is the more stable of the singlet states. The ground state of the molecule is calculated to be a triplet. This is somewhat surprising since the metal is surrounded by a strong σ ligand field. The fact that the triplet is the most stable structure results from the strong role that π-bonding has to play in determining the structures of these intermediates. It is significant for the discussion of the influence of π-bonding on the structure of an ML_4 complex that the three optimised structures are found on the C_{2v} energy surface.

In Figure 7 the frontier levels of each optimized structure are shown. Starting with the pseudotetrahedral singlet, on the left-hand side the expected two-below-three splitting pattern for the tetrahedron is absent. The 5-fold degeneracy of the d orbitals has been split by the ligand environment into an a_1 orbital lying below a group of three orbitals, a_2, b_1 and b_2, which in turn lie below another a_1 orbital.

The orbital contributions to these molecular orbitals are illustrated in Figure 8. In a pure tetrahedral field, based solely on σ-interactions, the e set comprises the d_{z^2} and d_{xy} orbitals (following the coordinate system shown in Figure 8). For the $[Fe(CO)_2(O)_2]$ molecule in such a geometry, these are still the lowest lying orbitals, but the d_{z^2} orbital lies at a considerably lower energy than the d_{xy} orbital. Distorting the molecule from a tetrahedron to a C_{2v} structure allows for mixing between some

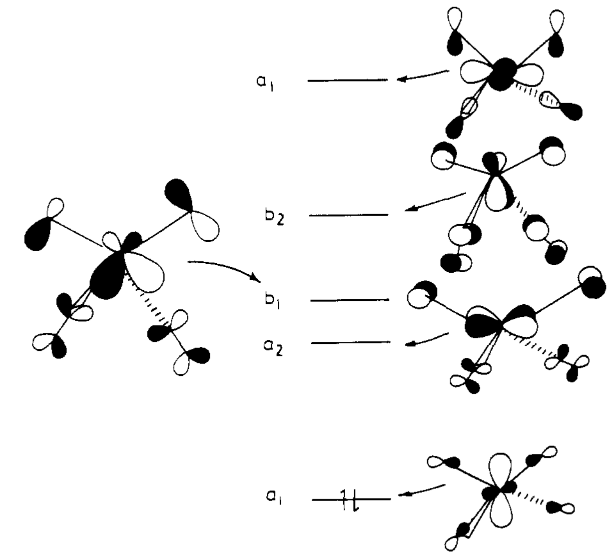

Figure 8. Molecular orbitals of the $[Fe(CO)_2(O)_2]$ singlet structure.

of the iron 3d orbitals and the 4p orbitals. In the case of the $1a_1$ orbital, the d_{z^2} and p_z orbitals mix. The a_2 orbital, predominantly d_{xy} on the metal, is a σ-innocent orbital. The π interactions are with the π^* orbitals of the carbonyls and the π orbitals of the oxo ligands. The contributions from the CO π^* orbitals to the a_2 molecular orbital are small. Although the π^* orbitals are in-phase with the d_{xy} orbital, the size of their contributions, together with the angular distribution of the carbonyl ligands, means that the overlap between the carbonyls and the d_{xy} orbital is small. In the case of the oxo ligands, the same applies except that now the contribution is larger, and the angular distribution is more favorable for overlap. Since the oxo ligands overlap out of phase, they have a destabilizing effect on the d_{xy} orbital. The arrangement of the ligands precludes σ interactions, and minimizes any π interactions. To whatever extent the π interactions affect the energy of the d_{xy} orbital, they do so in a destabilizing fashion. Above the a_2 orbital lie the b_1 and b_2 orbitals. These were formerly members of the t_2 set in T_d symmetry, but here they are stabilized with respect to the remaining member of the t_2 set, the $d_{x^2-y^2}$ orbital (a_1). The metal contribution to the b_1 orbital comes from a hybrid of the d_{xz} and p_x orbitals. This hybridization has resulted in a localization of the metal component in the region between the carbonyl ligands. Referring to Figure 8 shows that the carbonyl orbitals are in-phase with the metal orbital. The larger angle between the oxo ligands allows an in-phase overlap to occur between the oxo ligands and the metal. Without these stabilizing interactions the orbital would lie higher in energy.

Clearly the proximity in energy of the three orbitals, a_2, b_1 and b_2, is conducive to a high-spin configuration. The optimized triplet state, $^3B_1$, is 39.2 kJ mol^{-1} more stable than the singlet state just considered above. Comparing the two structures shown in Figure 6 and the molecular orbitals shown in Figure 7 shows that only a slight distortion of the geometry is necessary to reach the most stable triplet geometry. The distortion lowers the energy of the $b_2\alpha$ spin orbital below that of the $b_1\beta$ spin orbital. Beyond this point on the energy surface from a tetrahedron to a square plane, only one other minimum was located corresponding to a singlet of almost square planar geometry. This distortion has little effect on the energy of the a_1 orbital. The pseudo square planar singlet is calculated to be 49.6 kJ mol^{-1} less stable than the triplet and 10.4 kJ mol^{-1} less stable than the other pseudotetrahedral singlet.

The thermodynamics of this stage of the reaction were calculated for the transformations from $[Fe(CO)_4(O)_2)]$ to $[Fe(CO)_3(O)_2]$ and $[Fe(CO)_4(O_2)]$ to $[Fe(CO)_2(O)_2]$. The enthalpy change for $[Fe(CO)_4(O_2)]$ to $[Fe(CO)_3(O)_2]$ was calculated by considering the difference in energy of the ground state of $[Fe(CO)_4(O_2)]$ and the ground state of the system $[Fe(CO)_3(O)_2]$ and a free carbon monoxide molecule. For the purposes of calculating the ground-state energy of the latter system the carbonyl ligand was placed on the x-axis, at a distance of 30 Å from the central metal. A decomposition of ΔH into various components as before was not possible because of the obvious complexity of the reaction step depicted by eq 5 which involves the cleavage of a dioxygen bond and a metal–carbonyl bond. By this method we find the overall energy change to be 172.1 kJ mol^{-1}. This is higher than the previous bond cleavage step, a result to be expected since the bond breakages are more numerous. The bond cleavage of the carbonyl is compensated by the formation of two Fe=O bonds. The enthalpy change for $[Fe(CO)_4(O_2)]$ to $[Fe(CO)_2(O)_2]$ was calculated in a similar manner. For the purposes of calculating the ground state of the $[Fe(CO)_2(O)_2]$ + 2CO system, the carbonyl ligands were placed along the z-axis, in a positive and negative direction, respectively, at a distance of 30 Å from the central metal. The enthalpy change was calculated to be 196.3 kJ mol^{-1}.

$$Fe(CO)_4(O_2) \xrightarrow{\Delta H} Fe(CO)_3(O)_2 + CO \qquad (5)$$

$[Fe(CO)(O)_2]$. The third intermediate characterized on the basis of the experimental data by Fanfarillo *et al*[8] was $[Fe(CO)(O)_2]$, derived from $[Fe(CO)_3(O)_2]$ by the loss of two carbon monoxide molecules. According to spectroscopic evidence, the molecule is planar with a structure intermediate between T-shaped and trigonal planar. The $[Fe(CO)(O)_2]$ molecule has a choice between three classical planar three-coordinate structures, namely, T-shaped, trigonal planar or Y-shaped (see **4**).

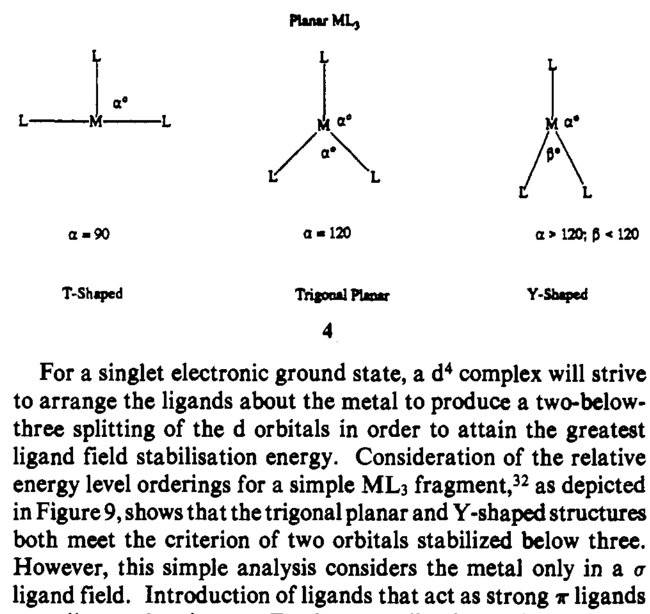

4

For a singlet electronic ground state, a d^4 complex will strive to arrange the ligands about the metal to produce a two-below-three splitting of the d orbitals in order to attain the greatest ligand field stabilisation energy. Consideration of the relative energy level orderings for a simple ML_3 fragment,[32] as depicted in Figure 9, shows that the trigonal planar and Y-shaped structures both meet the criterion of two orbitals stabilized below three. However, this simple analysis considers the metal only in a σ ligand field. Introduction of ligands that act as strong π ligands complicates the picture. Further complications arise when the molecule simultaneously contains π-acceptor ligands and π-donor ligands. The $[Fe(CO)(O)_2]$ molecule will strive to arrange the carbonyl and oxo ligands in such a manner as to produce a splitting of the metal d levels that leads to the greatest stabilization for a d^4 electronic configuration. The $[Fe(CO)(O)_2]$ molecule was optimised in the C_{2v} point group. The optimized structure for a closed shell configuration is shown in Figure 10.

The singlet electronic state geometry is seen to be intermediate between a T-shape and a trigonal plane. The angle between the oxo ligands is 140° with a reasonably short r(Fe–O) distance of 1.55 Å. The metal carbonyl distance, r(Fe–C), is 1.80 Å with the r(C–O) distance being 1.14 Å. This structure is very similar to the geometry proposed by Fanfarillo *et al.* on the basis of spectroscopic data.

The structure may be rationalized only by considering all the bonding features involved. Illustrations of the orbitals, together

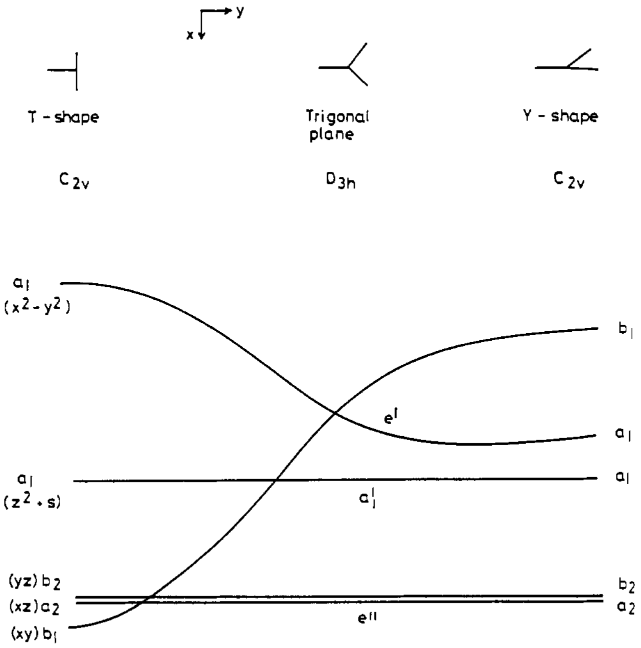

Figure 9. Molecular orbital correlation diagram for the interconversion of an ML_3 complex with T-shaped geometry to Y-shaped geometry via a trigonal planar structure.

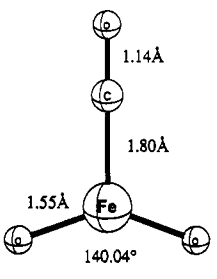

Figure 10. Optimized structure for $[Fe(CO)(O)_2]$.

with the energies of the frontier orbitals, are given in Figure 11. The d^4 electrons reside in the b_1 and $1a_1$ molecular orbitals of the molecule. These are composed of 83% d_{xz} in the former case and 90% $d_{z^2}/d_{x^2-y^2}$ hybrid in the latter case. Lying directly above these orbitals are the d_{yz}, d_{xy} and $d_{x^2-y^2}$ set, in that order. There are several interesting features about this energy level ordering. First, for the simple ML_3 case illustrated in Figure 9, the d_{xy} orbital is always the most stable d component since it is orthogonal to the plane of the molecule. In the $[Fe(CO)(O)_2]$ molecule, however, the d_{xy} orbital represents the second highest level. To understand the various orderings of the energies of the d orbitals of the metal, the contributions to the energy of each orbital are divided into two groups depending on whether they contribute to σ or to π interactions.

The d_{xz} orbital lies perpendicular to the plane of the molecule and therefore all the valence σ orbitals on the ligands lie in its nodal planes. Obviously there are no σ contributions to the energy of this orbital. Each ligand possesses two π orbitals which for reasons of clarity are denoted as $\pi_\perp$ and $\pi_\parallel$ ($\pi^*_\perp$ and $\pi^*_\parallel$ in the case of the carbonyl ligand) depending on whether they lie perpendicular or parallel to the plane of the molecule. The d_{xz} orbital can interact strongly with the $\pi^*_\perp$ orbital of the carbonyl and is stabilized by the resulting backbonding. For this geometry there is also the possibility of overlap with the $\pi^*_\perp$ orbitals on each of the oxo ligands. The overlap will not be as strong as the overlap with the $\pi^*_\perp$ orbital of the carbonyl since the angular arrangement is not optimal for maximum overlap. Consequently, although the interaction with the oxo groups is potentially destabilizing, it does not outweigh the stability conferred on the d_{xz} orbital by the carbonyl ligand. These interactions are shown in **5**.

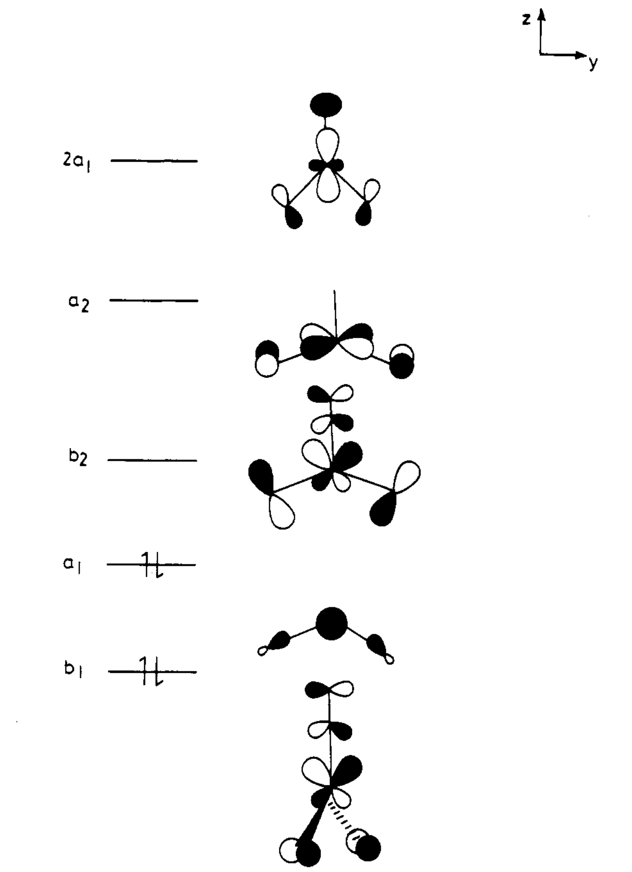

Figure 11. Molecular orbital diagrams and energies of the frontier energy levels of $[Fe(CO)(O)_2]$.

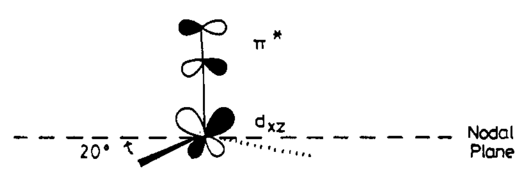

5

The d_{yz} orbital, coplanar with the molecule, is affected by the lone pairs in the σ orbitals of the oxo ligands. However, as illustrated in **5**, the oxo ligands are not located at the angle for maximum σ overlap with the d_{yz} orbital. There are also π interactions to consider. As with d_{xz} and the carbonyl $\pi^*_\perp$ orbital, the d_{yz} orbital has a large overlap with the carbonyl $\pi^*_\parallel$ orbital but the overlaps with the oxo π orbitals are larger. The net result of the σ interactions and destabilizing π interactions makes the d_{yz} orbital less stable than the d_{xz} orbital.

The ligand σ orbitals also lie in the nodal plane of the d_{xy} orbital, and therefore we focus our attention on the π interactions involving this orbital. As shown in **6**, the d_{xy} orbital does not

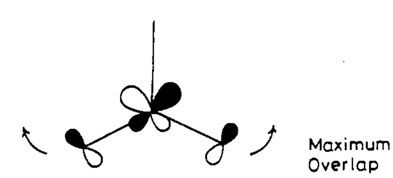

6

interact with the carbonyl ligand. Its sole interactions are with the $\pi_\perp$ orbitals of the oxo ligands. A T-shape geometry represents the best structure for maximum overlap between the d_{xy} orbital and the oxo $\pi_{\perp}$ orbitals. Movement of the ligands by 20° away from the T-shape and toward the trigonal planar structure will reduce the overlap. Nonetheless, because of the angular nature of the overlap, the diminution is not a rapid one, with the result that the d_{xy} orbital is still considerably destabilized with respect to its energy in the free metal atom.

Finally, the d_{z^2} and $d_{x^2-y^2}$ orbitals are considered together since in the C_{2v} point group these orbitals have the same symmetry and consequently mix to form hybrids. In the molecule these hybrids are the $1a_1$ and $2a_1$ orbitals.

So why does the geometry given in Figure 10 represent the minimum on the singlet state energy surface in C_{2v} symmetry? Is the singlet electronic state the ground state of the molecule? In the singlet structure the HOMO–LUMO gap is of the order of 1.2 eV. For a triplet to be stable it must distort the geometry in such a manner as to reduce the HOMO–LUMO gap. Qualitative predictions of the effects of geometric distortions on the energies of the metal orbitals may be made by inspecting the orbital diagrams given in Figure 11. The overlaps between the ligands and the metal for the b_2, a_2 and $2a_1$ orbitals suggest that a distortion to a T-shape would increase the energies of these orbitals with little effect on the b_1 and $1a_1$ orbitals. Distortions toward a trigonal plane suggest that the a_2 orbital would be stabilized, but the b_1 and $1a_1$ orbitals would also be stabilized. Qualitatively, therefore, it is difficult to envisage a triplet structure being more stable than the optimized singlet structure. The triplet structure was calculated to be 105 kJ mol^{-1} less stable.

Finally, we calculated the energy change for the loss of two carbonyl ligands from $[Fe(CO)_3(O)_2]$ to produce $[Fe(CO)(O)_2]$. The calculational method was the same as in the previous section whereby the enthalpy change is equivalent to the energy difference between the $[Fe(CO)_3(O)_2]$ intermediate and $[Fe(CO)(O)_2]$ with two carbon monoxide molecules 30 Å apart. The enthalpy change was calculated to be 80.4 kJ mol^{-1}. It is known for metal carbonyl complexes that the loss of a subsequent carbon monoxide molecule is more facile than the loss of the first carbon monoxide molecule. Thus, it is not so surprising that the dissociation energy for two carbon monoxide molecules from $[Fe(CO)_3(O)_2]$ is small. The value for the enthalpy change also agrees with the observation made by Fanfarillo *et al.*[8] that the $[Fe(CO)_3(O)_2]$ molecule fragments easily.

Final Stages of Oxidation. The fourth iron carbonyl intermediate detected in the reaction, E, was assigned as [Fe(CO)(O)], and is derived from $[Fe(CO)_3(O)_2]$. This assignment is a tentative one, based on the limited spectroscopic data available; the species is invariably formed only in low concentration and in the presence of more abundant photoproducts. However, such a species is not unprecedented, and other monooxo–iron species have been detected in photooxidation processes.[40] Attempts to find the ground-state electronic structure of this molecule proved to be very difficult. Like other highly unsaturated, electron-deficient molecules (e.g. $Ni(CO)$[41]), the ground-state electronic structure is very complex, invariably being high-spin. Taking the molecule to lie along the z axis, the d orbitals will be split as d_{z^2}, d_{xz}/d_{yz} and $d_{xy}/d_{x^2-y^2}$ in order of decreasing energy. We proceeded to perform calculations for all the possible high-spin states obtained by filling the five metal orbitals with six electrons. Eventually we found the most stable ground state for this molecule to be a triplet ($^3\Delta$). However, we also found another state only 1.3 kJ mol^{-1} less stable than the triplet state. The energy level diagrams are presented in Figure 12. The optimized geometry of the $^3\Delta$ state is shown in Figure 13. The molecule is calculated to have very long metal–oxygen and carbon–oxygen bonds, and an extremely short metal–carbon bond. According to Fanfarillo, *et al.*, the ν(Fe═O) vibration is quite high in energy, suggesting a strongly bound oxo ligand. However, the optimized structure that we calculate for this molecule suggests that both the ν(Fe═O) and ν(C═O) modes should be found at energies lower than their normal values.

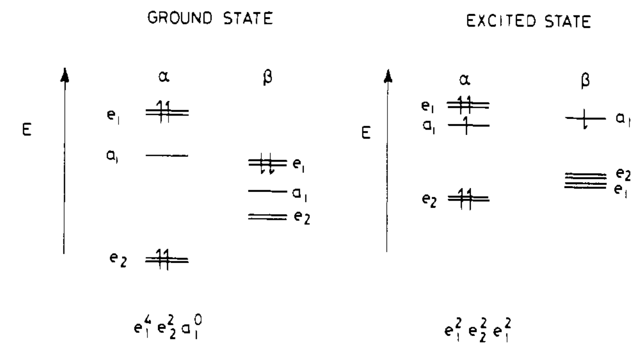

Figure 12. Energy levels for the two lowest energy states of [Fe(CO)(O)].

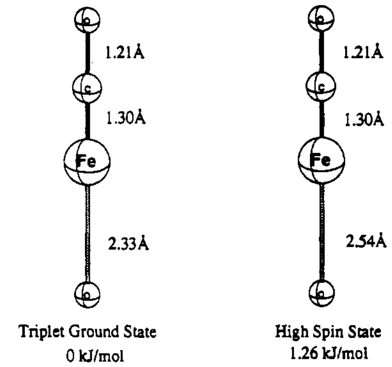

Figure 13. Optimized geometry of the [Fe(CO)(O)] ground and first excited state.

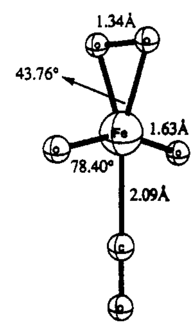

Figure 14. Optimized geometry of $[Fe(CO)(O)_2(O_2)]$.

The final carbonyl intermediate in the photooxidation of iron pentacarbonyl, F, was proposed to be $[Fe(CO)(O)_2(O_2)]$, the dioxygen adduct of the $[Fe(CO)(O)_2]$ intermediate. There are precedents for similar adducts being formed in photooxidation processes, as evinced by the formation of $(\eta^2\text{-}O_2)WO_2$ in the photooxidation of $W(CO)_6$.[7] One of the interesting features of the spectroscopic data is the remarkably high energy of the ν(C═O) vibration. Indeed, the wavenumber was reported to be in excess of that measured for free carbon monoxide, suggesting a weak linkage between the metal and the carbonyl ligand. Initially we searched for an optimal geometry for a closed-shell configuration, later investigating possible geometries for high-spin states. The geometry optimizations were performed in the C_s and C_{2v} point groups. We found that the closed shell configuration has a C_{2v} geometry which is depicted in Figure 14.

The $[Fe(CO)(O)_2]$ fragment is seen to have distorted from its ground state geometry (Figure 10), with the Fe═O bonds bending toward the carbonyl ligand by 11.5° from the horizontal. The dioxygen bond length has increased from its ground state value

(40) Kafafi, Z. H.; Hauge, R. H.; Billups, W. E.; Margrave, J. L. *J. Am. Chem. Soc.* **1987**, *109*, 4775.
(41) Walch, S. P.; Goddard, W. A., III *J. Am. Chem. Soc.* **1976**, *98*, 7908.

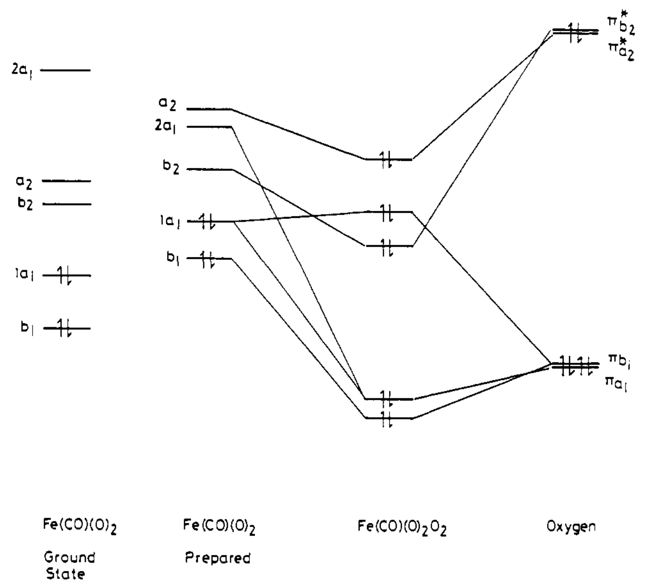

Figure 15. Fragment interaction diagram for $[Fe(CO)(O)_2(O_2)]$.

Table III. Contributions (kJ mol^{-1}) to ΔH for the addition of O_2 to $[Fe(CO)(O)_2]$[a]

$\Delta E°$	ΔE_{prep}	ΔE_{a_1}	ΔE_{b_1}	ΔE_{b_2}	ΔE_{orb}
635.0	177.7	−133.7	−617.1	−37.0	−921.3

[a] $\Delta E_{orb} = \Delta E_{a_1} + \Delta E_{b_1} + \Delta E_{b_2}$ including Becke and Perdew corrections.

of 1.16 Å to 1.34 Å, and the dioxygen bite angle is 43°. Such values are similar in magnitude to those found previously for $[Fe(CO)_4(O_2)]$. The most striking feature of the optimized geometry is the extremely long metal–carbonyl bond distance. At approximately 2.1 Å, this constitutes a very weak bond. The carbonyl bond distance, at 1.13 Å, is shorter than that of any other carbonyl distance computed in these calculations. Certainly, therefore, with respect to metal–carbonyl bonding, the optimised structure agrees with the experimental description of the intermediate. The source of the interesting geometrical features may be found by considering the electronic structure of the complex. In Figure 15 we present the pertinent fragment interactions between $[Fe(CO)(O)_2]$ and dioxygen. On the left-hand side we show the evolution of the $[Fe(CO)(O)_2]$ frontier orbitals as the fragment distorts from its ground-state geometry to the geometry that it assumes in the molecule.

Distorting the $[Fe(CO)(O)_2]$ fragment raises the energies of the frontier orbitals. These energy changes are to be expected considering the nature of the overlaps of the metal orbitals with the ligand orbitals, as depicted in Figure 11. Lengthening the metal–carbonyl bond has limited the benefits of back-bonding to the π^* orbital of this ligand, while bending back the oxo ligands increases the interactions between the oxo groups and the metal orbitals. The interaction energies for each orbital type are presented in Table III. The main interaction is between the $\pi^*_{b_1}$ orbital of oxygen and the d_{xz} orbital of the metal fragment. The interaction diagram is similar to that found for $[Fe(CO)_4(O_2)]$.

The calculation of the enthalpy change for

$$[Fe(CO)(O)_2] + O_2 \xrightarrow{\Delta H} [Fe(CO)(O)_2(O_2)] \qquad (6)$$

was performed in the same way as for $[Fe(CO)_4(O_2)]$ using eq 4. In this instance $\Delta E°$ refers to the steric repulsion between $[Fe(CO)(O)_2]$ and dioxygen and ΔE_{prep} is the energy required to raise $[Fe(CO)(O)_2]$ from its ground state to the geometry that it adopts in $[Fe(CO)(O)_2(O_2)]$, with a singlet electronic configuration. Additionally, ΔE_{prep} includes the energy needed to promote dioxygen from its ground-state configuration $^3\Sigma_g^+$ $[(\pi^*_{b_1})^1(\pi^*_{a_2})^1]$ and equilibrium bond distance to the electronic configuration $[(\pi^*_{b_1})^0(\pi^*_{a_2})^2]$ with a bond distance equivalent to the O_2 distance in $[Fe(CO)(O)_2(O_2)]$. The values for the various components of eq 4 are given in Table III.

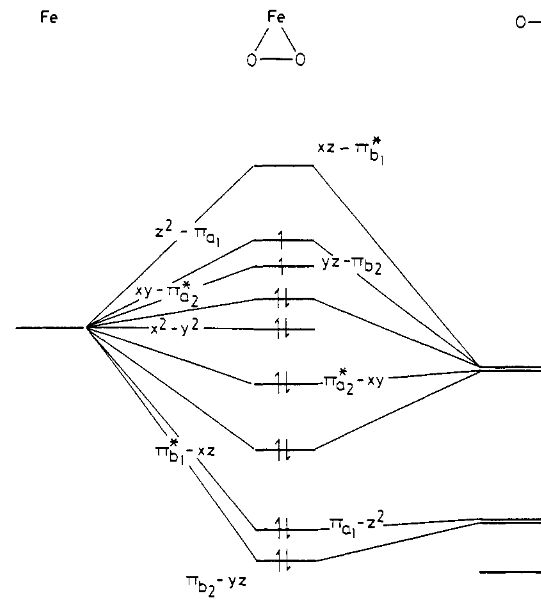

Figure 16. Frontier orbital interaction diagram for $[Fe(\eta^2\text{-}O_2)]$.

Initial Binary Oxide: Iron Dioxide. Fanfarillo *et al.*[8] report the detection of $[Fe(\eta^2\text{-}O_2)]$ as the first binary oxide to be formed in the photooxidation of $[Fe(CO)_5]$. This peroxo form of FeO_2 has been detected previously in matrix-isolation studies,[42] as indeed has the dioxo form $[Fe(O)_2]$, although there are some inconsistencies between the results and between the interpretation of different experiments.[43] We explored the $[Fe(\eta^2\text{-}O_2)]$ and $[Fe(O)_2]$ energy surfaces to locate the respective ground states.

$[Fe(\eta^2\text{-}O_2)]$. This is the structure that has been proposed by Griffith[44] for dioxygen coordination to hemoglobin. It is also the structure proposed for the matrix product detected by Fanfarillo *et al.* The interaction diagram for the frontier orbitals of iron and the oxygen molecule are shown in Figure 16. From the d manifold of iron only the $d_{x^2-y^2}$ orbital remains nonbonding in the molecule. All the other d orbitals interact to varying degrees with the frontier orbitals of dioxygen. The main interaction is between the d_{xz} and $\pi^*_{b_1}$ orbitals. Hence the π^* orbitals of dioxygen are split. The d_{xy} and $\pi^*_{a_2}$ orbitals overlap in δ fashion and thus the interaction is not as strong as that between d_{xz} and the $\pi^*_{b_1}$ orbitals. The d_{yz} and π_{b_2} orbitals overlap weakly, as do the d_{z^2} and π_{a_1} orbitals. These interactions are depicted in 7. The

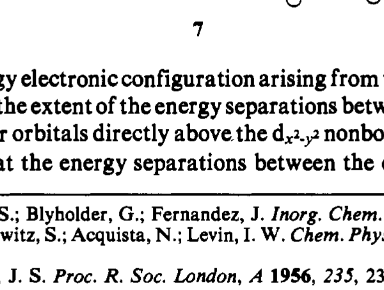

7

lowest energy electronic configuration arising from these overlaps depends on the extent of the energy separations between the group of molecular orbitals directly above the $d_{x^2-y^2}$ nonbonding orbital. We find that the energy separations between the $d_{xy} - \pi^*_{a_2}$, d_{yz}–

(42) Chang, S.; Blyholder, G.; Fernandez, J. *Inorg. Chem.* **1981**, *20*, 2813.
(43) Abramowitz, S.; Acquista, N.; Levin, I. W. *Chem. Phys. Lett.* **1977**, *50*, 423.
(44) Griffith, J. S. *Proc. R. Soc. London, A* **1956**, *235*, 23.

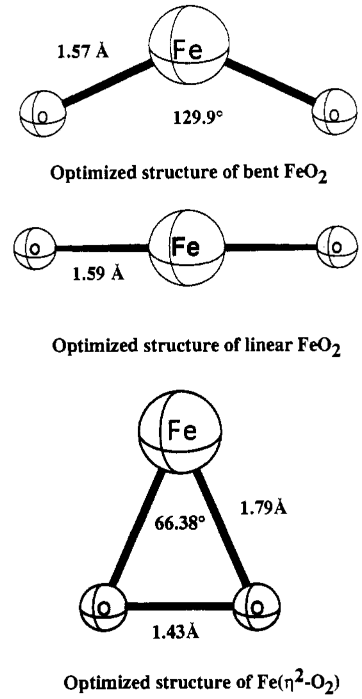

Figure 17. Ground-state geometries of [Fe(η^2-O_2)] and linear and bent [Fe(O)$_2$].

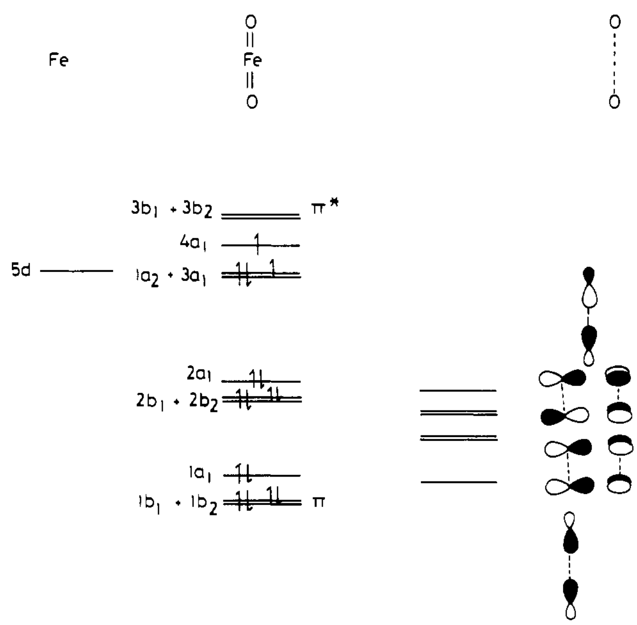

Figure 18. Frontier orbital diagram of linear [Fe(O)$_2$].

π_{b_2}, and d_{z^2}–π_{a_1} molecular orbitals are too small to sustain a singlet ground-state electronic configuration. Instead we find the ground state to be $^3B_2$, with the δ molecular orbital, $d_{xy} - \pi^*_{a_2}$, doubly occupied and with d_{z^2}–π_{a_1} and d_{yz}–π_{b_2} each singly occupied. The geometry of the ground state is shown in Figure 17.

Linear [Fe(O)$_2$]. Molecular orbital calculations on linear [Fe(O)$_2$] were performed in the C_{2v} point group. The orbital interaction diagram is shown in Figure 18. The linear combinations of the oxo valence orbitals, which are shown on the right hand side of Figure 18, comprise in-phase and out-of-phase σ and π combinations of the oxygen p orbitals. The out-of-phase π set combines with the metal d_{xz} and d_{yz} orbitals to form the π bonds of the molecule. The in-phase π combination of oxo ligands does not find a match with the metal d orbitals and remains nonbonding. The in-phase σ combination of the oxo ligands overlaps with the metal d_{z^2} orbital to form the Fe–O σ bonds. The out-of-phase σ combination of the oxo ligands also has a_1 symmetry and mixes

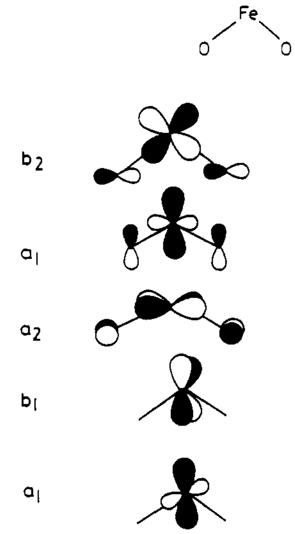

Figure 19. Frontier orbitals of bent [Fe(O)$_2$].

with the d_{z^2} orbital. However, this interaction is nonbonding and results in the $1a_1$ and $4a_1$ orbitals of the molecule. The former is essentially ligand-based while the $4a_1$ orbital is centered on the metal. The ground-state electronic configuration is determined by the relative energies of the three metal-based nonbonding orbitals, $1a_2$, $3a_1$ and $4a_1$. Occupying these orbitals with the remaining four valence electrons of this Fe(IV) complex may result in either a singlet or a triplet ground state. We find the triplet state, $^3B_2$, to be more stable, and the optimized geometry for this electronic state is shown in Figure 17.

Bent [Fe(O)$_2$]. Bending the bond angle of this compound from 180 to 130° gives rise to another minimum in the potential energy surface; the optimized structure is shown in Figure 17. The frontier molecular orbitals of [Fe(O)$_2$] with a bent geometry are shown in Figure 19. The arrangement of the oxo ligands gives rise once again to two essentially non-bonding metal-based orbitals. These are the d_{yz} orbital and a hybrid of d_{z^2} and $d_{x^2-y^2}$ orbitals. Above these orbitals lie an a_2 and a_1 orbital. The a_2 orbital is the antibonding component of the interaction between the d_{xy} orbital and the π^* combination of oxo p orbitals. These orbital interactions give rise to a $^3B_2$ ground state.

We have presented in this section the optimized ground-state geometries for the three forms of FeO_2 that have been identified in different matrix-isolation experiments.[8,42,43] The dioxo compounds are much more stable than the peroxo form. For each of the geometries there are other minima on the energy surface corresponding to higher energy electronic configurations. In a future detailed study of the electronic interactions of iron with dioxygen, we shall explore the features of these higher lying electronic states, together with other alternative models of iron–dioxygen interaction in relation to the structure of the complex formed between dioxygen and hemoglobin.[45]

Final Product: Iron Trioxide. The prolonged photooxidation of [Fe(CO)$_5$] in an argon matrix results in the production of [FeO$_3$] as the final product.[8] Once again on the basis of the infrared spectrum, it is proposed that [FeO$_3$] has a D_{3h} geometry, isostructural with the previously characterized d^0 MoO_3[46] and WO_3[47] species. Additionally, the structure resembles that reported recently by Schrock *et al.*[48] for Os(NAr)$_3$. Although oxo products of iron(VI) such as FeO_4^{2-} have been known for a long time, [FeO$_3$] represents the first characterization of a binary iron(VI)

(45) (a) Shaanan, B. *Nature* **1982**, *296*, 683. (b) Jameson, G. B.; Molinaro, F. S.; Ibers, J. A.; Collman, J. P.; Brauman, J. I.; Rose, E.; Suslick, K. S. *J. Am. Chem. Soc.* **1980**, *102*, 3224. (c) Yamamoto, S.; Kashiwagi, H. *Chem. Phys. Lett.* **1989**, *161*, 85 and references therein.
(46) Hewett, W. D., Jr.; Newton, J. H.; Weltner, W., Jr. *J. Phys. Chem.* **1975**, *79*, 2640.
(47) Green, D. W.; Ervin, K. M. *J. Mol. Spectrosc.* **1981**, *89*, 145.

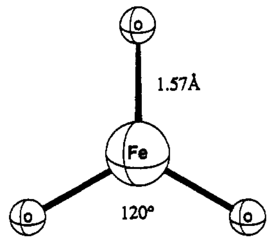

Figure 20. Ground-state-optimized geometry of $[FeO_3]$. The optimization was performed in the C_{2v} and C_{3v} point groups.

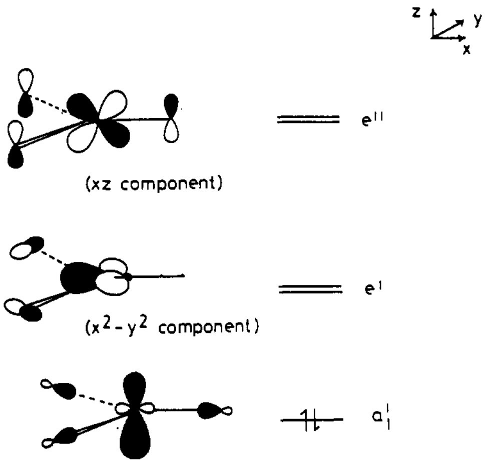

Figure 21. Frontier orbitals of the $[FeO_3]$ molecule.

compound. The geometry of $[FeO_3]$ was optimized in C_{2v} and C_{3v} symmetries to determine if the molecule relaxes either to a distorted planar or to a pyramidal structure. Extensive searches within these symmetries did not yield any reason to suggest that $[FeO_3]$ adopts other than a trigonal planar geometry in the ground state. The fully optimized geometry is illustrated in Figure 20. The iron–oxygen bond length is calculated to be 1.57 Å. In Figure 21 we depict the frontier orbitals of $[FeO_3]$.

The lowest lying metal orbital, $5a_1'$, is seen to be predominantly d_{z^2} in character with a slight admixture of s. This orbital is perpendicular to the plane of the molecule and therefore interacts only slightly with the σ lone pair orbitals of oxygen. In fact, admixture of the iron s orbital has further reduced the destabilizing interaction with the oxygen long pairs. The next set of metal orbitals is the e′ set, comprising mainly the d_{xy} and $d_{x^2-y^2}$ orbitals. These enter into π interactions with the ligand orbitals, with σ interactions having a much smaller influence. The trigonal planar geometry of the molecule prevents large destabilization of these orbitals by σ interactions. In addition, the geometry imposes destabilizing interactions with the $\pi_{\parallel}$ orbitals of the ligands, thus causing the d_{xy} and $d_{x^2-y^2}$ orbitals to be higher in energy relative to the d_{z^2} orbital. The remaining d orbitals of the metal, d_{xz} and d_{yz} (e″), are destabilized the most by the strong overlaps with the oxygen ligands. There is no σ contribution to the energies of these orbitals since the molecular plane is coincident with one of the nodal planes of the orbitals.

Having identified the valence d orbitals of the metal and rationalized their ligand field splittings, we may now draw attention to the second highest occupied orbital, a_2. This orbital is entirely centered on the ligand atoms. Thus, if the molecule is considered as a d^2 species, the valence electron count of 20 is not strictly accurate, since two of the electrons reside exclusively among the ligand atoms. This is also the case for $Os(NAr)_3$ as determined by SCF–Xα SW calculations.[48] These seemingly electron-supersaturated systems, although not very common, are well documented. Some of the more familiar examples are $Zr(BH_4)_4$,[49] $W(C_2H_2)CO$,[50] MCp_3, and MCp_3X (M = lanthanide or actinide metal),[51] and Hoffmann *et al.*[52] have studied the influence of these ligand-based electron sinks on reactivity. Such "valence-expanded" molecules arise from the symmetry of the problem. It is possible to determine for a particular molecule the number and type of ligand-based orbitals that are nonbonding, once the point group of the molecule is known. So $[FeO_3]$, with its valence-expanded electronic structure, is but an example of a class of molecules that accommodate electrons in excess of the 18 electron rule in ligand-based orbitals. We have shown that for a D_{nh} system the number of nonbonding orbitals can be deduced. This treatment can be extended to all point groups.[53]

Finally, we calculated the enthalpy change for the process

$$Fe(CO)(O)_2(O_2) \xrightarrow{\Delta H} FeO_3 + CO_2 \qquad (7)$$

Although the scheme proposed by Fanfarillo *et al.* allows for the generation of iron trioxide by an alternative route via [Fe(CO)(O)], the route indicated above is the more favorable, and since the complexity of the electronic structure of [Fe(CO)(O)] is not easily amenable to an enthalpy calculation, we feel that the above process is the better choice for this work. The energy change was calculated as 165.0 kJ mol^{-1}.

Conclusions

The main purpose of this work was to ascertain the ground-state electronic configurations and geometries of the various molecules observed by Fanfarillo *et al.*[8] during the photooxidation of $[Fe(CO)_5]$ in an argon matrix. In addition to characterizing the structures of the $Fe(CO)_x(O)_y$ intermediates, we have calculated the energy changes from reactants to products. The optimized geometries of this work agree well, for the most part, with the geometries proposed by Fanfarillo *et al.* on the basis of infrared spectroscopic analyses. The identification strategy used by Fanfarillo *et al.* was to treat each molecule in terms of $Fe(CO)_x$ and $Fe(O)_y$ component fragments. By studying the number, energies and relative intensities of the ν(CO) absorptions, performing several isotopic enrichment experiments, and comparing the experimental and calculated results for various $Fe(CO)_x$ fragments, they were able, with varying degrees of assurance, to assign a local symmetry to the $Fe(CO)_x$ fragment. For the $Fe(O)_y$ fragments, the coordination mode of oxygen was determined by reference to the effects of ^{18}O enrichment. It is much more difficult, however, to determine the relative disposition of the $Fe(CO)_x$ and $Fe(O)_y$ components. A comparison of the structures calculated here with those proposed by Fanfarillo *et al.* shows remarkable agreement in the *local* symmetries of the $Fe(CO)_x$ and $Fe(O)_y$ fragments of each molecule.

Nonetheless, there are discrepancies between the calculated and experimentally proposed structures. This is most evident for [Fe(CO)(O)], which in experimental terms is one of the least well characterized molecules of the photooxidation process. An important potential source of discrepancies is the role played by the matrix in influencing the geometry of a particular molecule.[54] The optimized geometries presented here are for the free molecule in the gas phase. The relative importance of host–guest interactions in determining the structure of a matrix-isolated

(48) Schofield, M. H.; Kee, T. P.; Anhaus, J. T.; Schrock, R. R.; Johnson, K. H.; Davis, W. M. *Inorg. Chem.* **1991**, *30*, 3595.

(49) (a) Bird, P. H.; Churchill, M. R. *Chem. Commun.* **1967**, 403. (b) Davison, A.; Wreford, S. S. *Inorg. Chem.* **1975**, *14*, 703.

(50) (a) Tate, D. P.; Augl, J. M.; Ritcbey, W. M.; Ross, B. L.; Grasselli, J. G. *J. Am. Chem. Soc.* **1964**, *86*, 3261. (b) King, R. B. *Inorg. Chem.* **1968**, *7*, 1044. (c) Laine, R. M.; Moriarty, R. E.; Bau, R. *J. Am. Chem. Soc.* **1972**, *94*, 1402.

(51) (a) Perego, G.; Cesari, M.; Farina, F.; Lugli, G. *Acta Crystallogr., B* **1976**, *32*, 3034. (b) Kanellakopulos, B.; Bagnall, K. W. *MTP Int. Rev. Sci., Inorg. Chem., Ser. 1* **1972**, *7*, 299.

(52) Chu, S.-Y.; Hoffmann, R. *J. Phys. Chem.* **1982**, *86*, 1289.

(53) Lyne, P. D.; Mingos, D. M. P. Unpublished results.

molecule increases along the scale Ne < Ar < Kr < Xe < N_2. The experimental work was performed with an argon matrix, and although argon is known to form reasonably inert matrices, the possibility that interactions with the matrix affect the structures of weakly bound, pliable guest molecules cannot be ruled out.

The importance of the molecules studied by Fanfarillo *et al.* cannot be overstated. Oxo–iron carbonyl complexes are likely to be intermediates in catalytic oxidation processes and carbonylation reactions.[1e,2,55] In addition, oxygen-binding to iron has a crucial role to play in biological processes. In principle, therefore, the structural and electronic characterization of these species represents a valuable contribution to the understanding of such processes.

Acknowledgment. We thank the AFOSR and the Natural Sciences and Engineering Research Council of Canada (NSERC) for financial support. P.D.L. expresses his gratitude to the British Council for a scholarship and all the members of the Ziegler group, in particular Heiko Jacobsen, for teaching him how to use the HFS program. All calculations were carried out on the computer installations at the University of Calgary.

(54) (a) Arthers, S. A.; Beattie, I. R.; Jones, P. J. *J. Chem. Soc., Dalton Trans.* **1984**, 711. (b) Beattie, I. R.; Millington, K. R. *J. Chem. Soc., Dalton Trans.* **1987**, 1521. (c) Beattie, I. R.; Jones, P. J.; Millington, K. R.; Willson, A. D. *J. Chem. Soc., Dalton Trans.* **1988**, 2759. (d) Ogden, J. S.; Levason, W.; Hope, E. G.; Graham, J. T.; Jenkins, D. M.; Angell, R. M. *J. Mol. Struct.* **1990**, *222*, 109. (e) Swanson, B. I.; Jones, L. H. *Vibrational Spectra and Structure*; Durig, J., Ed.; Elsevier, 1983; Vol. 12. (f) Horton-Mastin, A.; Poliakoff, M. *Chem. Phys. Lett.* **1984**, *109*, 587. (g) Demuynck, J.; Kochanski, E.; Veillard, A. *J. Am. Chem. Soc.* **1979**, *101*, 3467.

(55) Mimoun, H. In *Comprehensive Coordination Chemistry*; Wilkinson, G., Gillard, R. D., McCleverty, J. A., Eds.; Pergamon: Oxford, 1987; Vol. 6, p 317.